Seasonal variability of the potential vorticity in the Lofoten vortex

Elena V. Novoselova[1]

Received 10 January 2022; accepted 22 February 2022; published 16 June 2022.

The anticyclonic quasi-permanent Lofoten vortex is a strong dynamic formation in the center of the Lofoten Basin in the Norwegian Sea. We used the oceanic reanalysis data GLORYS12V1. We analyzed a seasonal distribution of the relative and potential vorticity, as well as the orbital velocities and the potential density in the Lofoten vortex. The main points of the potential vorticity calculating are considered. The values of the Lofoten vortex volume, the horizontal dimension (the diameter) as well as the vertical scale for the period from 2000 to 2019 are obtained, as well as the method for estimates of these characteristics is described in detail. It was shown that the intensification of the vortex occurs in the summer, and its relaxation – in the winter. *KEYWORDS:* North Atlantic; Norwegian sea; Lofoten basin; Lofoten vortex; potential vorticity; relative vorticity.

Citation: Novoselova, Elena V. (2022), Seasonal variability of the potential vorticity in the Lofoten vortex, *Russ. J. Earth. Sci., 22,* ES3006, doi:10.2205/2022ES000786.

1. Introduction

Potential Vorticity (PV) is often considered as the absolute circulation of a particle enclosed between two isentropic (for the atmosphere) or isopycnal (for the ocean) surfaces (Winkler, R., Zwatz-Meise, V., 2001, Manual of synoptic satellite meteorology. Conceptual models and case studies. Version 6.8. http://www.zamg.ac.at/docu/Manual). *PV* can also be calculated relative to surfaces of equal depth or pressure. Potential vorticity combines the dynamic effects of the Earth's rotation around its axis and the rotation of fluid elements around their centers. Thus, *PV* is a combination of the small-scale fluid properties and the large-scale dynamic variability. In practice, *PV* can be used to assess the lateral exchange at the outer vortex boundary [*Bosse et al.,* 2019].

The *PV* calculation is based on the Ertel theorem, which is also called the Ertel-Rossby theorem [*Allen and Smeed,* 1996], (Smith, R. K., 2003, Potential Vorticity, https://www.meteo.physik.uni-muenchen.de/lehre/roger/Adm_Lectures/PV.pdf), or the equation of potential vorticity conservation. It is often believed that Rossby and Ertel obtained their potential vorticity conservation laws independently, but according to [*Samelson,* 2003] this is not the case. His paper contains the rationale of this issue, we will mention the main points. In the article [*Rossby,* 1936] the Lagrangian conservation law for the shallow water model is derived. If we differentiate the equations of motion and neglect the terms multiplied by the vertical velocity component (w), but allow variations in latitude (f), we can get the well-known relationship (1) between vorticity (ζ) and horizontal divergence:

$$\frac{d\left(\zeta+f\right)}{dt}=-\left(\zeta+f\right)\left(\frac{\partial u}{\partial x}+\frac{\partial v}{\partial y}\right), \qquad (1)$$

where f is the Coriolis parameter (planetary vorticity);

[1]Saint Petersburg State University, Saint Petersburg, Russia

http://rjes.wdcb.ru/doi/2022ES000786-res.html

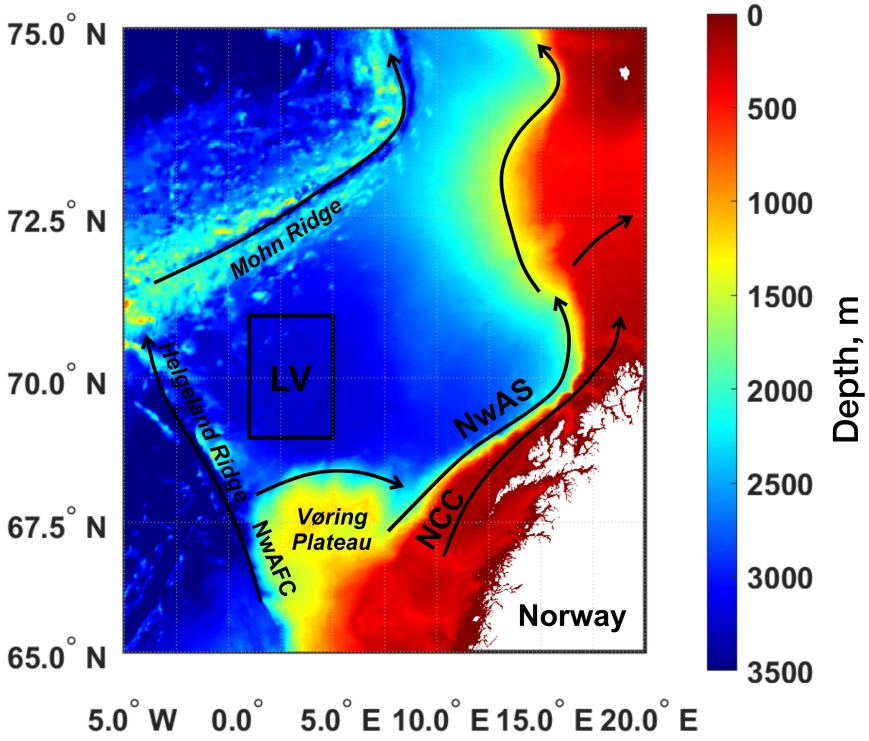

Figure 1. The Lofoten Basin. The color indicates the bottom topography (m). The arrows indicate the Norwegian Current branches: NwASC is the Norwegian Slope Current, NCC is the Norwegian Coastal Current, NwAFC is the Norwegian Frontal Current. The study area is marked with a rectangle, LV is the Lofoten Vortex.

$$\zeta = (\text{curl}\, V)_z = \frac{\partial v}{\partial x} - \frac{\partial u}{\partial y}$$

is the relative vorticity; t is the time; u, v are the zonal and meridional velocity components. Using the continuity equation (2) and eliminating the divergence, Rossby obtained the formula (3):

$$\frac{1}{D}\frac{dD}{dt} = -\left(\frac{\partial u}{\partial x} + \frac{\partial v}{\partial y}\right), \quad (2)$$

$$\zeta + f = cD, \quad (3)$$

where D is the thickness of a homogeneous liquid layer, $c$is the constant value for any individual column of liquid, which can vary from one trajectory to another. Rossby compared the constant c with the Bernoulli function in a steady flow and showed how the relative vorticity is related to the flow depth according to the conservation law. In the article [*Rossby,* 1938] author generalized the potential vorticity conservation law for a continuously stratified hydrostatic fluid. These findings are drawn in an alternative form in [*Rossby,* 1940], where the author introduced the term "potential vorticity". In 1942 Ertel published several short papers where he derived a set of potential vorticity theorems for ideal non-hydrostatic compressible fluids [*Ertel,* 1942a, 1942b, 1942c; *Schubert et al.,* 2004]. Ertel's results are more general than Rossby's and are formulated using vector calculus and the standard Eulerian vertical coordinate, while Rossby used quasi-Lagrangian, isopycnal, or isentropic surfaces.

The Lofoten Basin (LB) is located in the northern part of the Norwegian Sea and has a maximum depth of 3303 m according to the global elevation model ETOPO1 [*Amante and Eakins,* 2009]. It is surrounded by the Mohn and Helgeland Ridges from the west, the Vøring Plateau from the south, and the Norwegian coast from the east (Figure 1). The basin is surrounded by two branches of the Norwegian Current: the Norwegian Slope Current (NwASC) and the Norwegian Frontal Current

(NwAFC). The LB is a transit zone of warm Atlantic waters to the Arctic, where they accumulate and transform [*Koszalka et al.,* 2011; *Rossby et al.,* 2009b; *Ypma et al.,* 2020]. The energy vortex field of the basin redistributes these waters in the basin, resulting in large heat losses from the sea surface to the atmosphere [*Dugstad et al.,* 2021]. Due to this, LB is called the "heat reservoir" of the entire region *Rossby et al.,* 2009a]. On average, the depth of winter convection in the basin can reach from 600 m [*Bashmachnikov et al.,* 2017b; *Nilsen and Falck,* 2006; *Raj et al.,* 2015; *Volkov et al.,* 2015] up to 800 m [*Bosse et al.,* 2018; *Köhl,* 2007; *Søiland et al.,* 2016; *Søiland and Rossby,* 2013]. In the case of especially intense convective processes (for example, in the winter of 2009–2010), the depth of the mixed layer depth can reach up to 1000 m [*Bosse et al.,* 2018; *Fedorov et al.,* 2019, 2021; *Spall,* 2010].

The main feature of the LB is the quasi-permanent anticyclonic Lofoten Vortex (LV). It is a convective lens of warm and salty water at a depth of 300–1000 m with a spatial scale of about 100 km [*Bashmachnikov et al.,* 2017a; *Bashmachnikov et al.,* 2017b*Belonenko et al.,* 2017, 2018; *Ivanov and Korablev,* 1995a, 1995b]. The eddy is also identified as an area of the local level rise and increased kinetic energy of currents [*Bashmachnikov et al.,* 2017a; *Belonenko et al.,* 2014; *Köhl,* 2007; *Volkov et al.,* 2015]. Winter convection [*Alexeev et al.,* 2016; *Bloshkina and Ivanov,* 2016; *Fedorov et al.,* 2019; *Ivanov and Korablev,* 1995a, 1995b; *Novoselova and Belonenko,* 2020; *Travkin and Belonenko,* 2020; *Yu et al.,* 2017] and/or merging with other mesoscale eddies breaking away from the Norwegian Current [*Fedorov and Belonenko,* 2020; *Fer et al.,* 2018; *Gordeeva et al.,* 2020; *Köhl,* 2007; *Travkin and Belonenko,* 2019; *Trodahl et al.,* 2020; *Zinchenko et al.,* 2019] are considered to be the main reasons for vortex regeneration. The vertical thickness of the core formed during convection is determined by its pre-convective thickness, heat transfer intensity in the winter season, and horizontal heat advection [*Ivanov and Korablev,* 1995b]. Also, the bowl-shape bottom of the basin significantly reduces the rate of LV destruction [*Bashmachnikov et al.,* 2017b; *Belonenko et al.,* 2021]. Model experiments in the article [*Santeva et al.,* 2021] showed that the vortex lifetime significantly depends on its position in the basin, the bottom topography, and the speed of the incident flow: the greater the incident flow speed and the shallower the depression depth in the basin center, the faster the vortex is destroyed. In addition, mesoscale cyclones surrounding the LV isolate it from the external environment and contribute to its stabilization [*Raj et al.,* 2020].

According to the articles [*Belonenko et al.,* 2014; *Ivanov and Korablev,* 1995b], LV is most intensive in winter when the thermohaline anomalies intensify so the eddy shrinks to the baroclinic Rossby radius (7–9 km [*Chelton et al.,* 1998; *Novoselova et al.,* 2020]) and anticyclonic vorticity increases. In summer, the vortex relaxes, its horizontal dimensions increase and the speed of orbital motion decreases [*Alexeev et al.,* 2016; *Belonenko et al.,* 2014; *Ivanov and Korablev,* 1995b].

2. Methods

2.1. Potential Vorticity Calculation

The Rossby potential vorticity conservation law (4) combines the change in depth (H), relative vorticity (ζ) and latitude (namely, the Coriolis parameter f), and was obtained in [*Rossby,* 1940]:

$$\frac{d}{dt}\left(\frac{\zeta + f}{H}\right) = 0. \tag{4}$$

The value in parentheses is called the potential vortex (PV) and is constant along the flow path (formula (5)):

$$PV = \frac{\zeta + f}{H} = \text{const}. \tag{5}$$

Firstly, a flow thickness variation leads to a change in the relative vorticity. Consider the example in Figure 2. The liquid column is limited by two isosurfaces, for example, isopycnal. Since the potential density is conserved as the liquid column moves, it stretches or shrinks as the thickness changes between the isopycnal surfaces. Since the mass

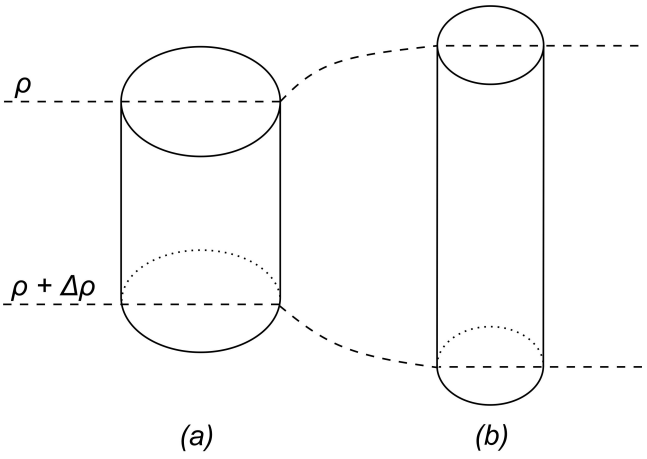

Figure 2. The illustration of the potential vorticity conservation.

of the liquid column is also being the same, vertical stretching reduces the column base area and vice versa. As a result, when the vortex expands (Figure 2, movement from "b" to "a"), its rotation slows down, and when the vortex converges horizontally (Figure 2, movement from "a" to "b"), the speed increases to maintain potential vorticity [*Kushner,* 2003; *Talley et al.,* 2011]. In literature, for example [*Steele et al.,* 2001; *Stewart,* 2008; *Vallis,* 2006], this phenomenon is often compared to the rotation of an ice skater, whose rotation slows down when her arms are spread out and increases when she is stretched up. We will refer to this as the "ice skater effect". Secondly, a change in latitude requires a corresponding shift in the relative vorticity: as the water column approaches the equator, the planetary vorticity f decreases, while the relative vorticity ζ, on the contrary, increases [*Stewart,* 2008]. Note that PV remains the same in the absence of mixing with other particles or friction losses [*Catling,* 2015; *Pidcock et al.,* 2013]. The PV change means that diabatic processes are involved: the release of latent heat, friction, radiation, etc.

The articles [*Zhmur et al.,* 2021a, 2021b, 2022] contain a detailed description of the methods for calculating Ertel's and Rossby's potential vorticity. In this paper, we will use Ertel's potential vorticity. Let us consider further only the main points. In general, the for a baroclinic flow in a stratified fluid will be calculated by the formula (6) in vector form and the formula (7) in the scalar form [*Allen and Smeed,* 1996; *Stewart,* 2008], (Smith, R. K., 2003, Potential Vorticity, https://www.meteo.physik.uni-muenchen.de/lehre/roger/Adm_Lectures/PV.pdf):

$$PV = \frac{\boldsymbol{\omega} + 2\,\boldsymbol{\Omega}}{\rho} \times \nabla\lambda, \tag{6}$$

$$PV = \frac{1}{\rho}\left(\left(\frac{\partial w}{\partial y} - \frac{\partial v}{\partial z}\right)\frac{\partial \lambda}{\partial x} + \right.$$

$$\left.\left(f_h + \frac{\partial u}{\partial z} - \frac{\partial w}{\partial x}\right)\frac{\partial \lambda}{\partial y} + (f+\zeta)\,\frac{\partial \lambda}{\partial z}\right), \tag{7}$$

where $\boldsymbol{\omega}$ and $2\,\boldsymbol{\Omega}$ are the relative and planetary vorticity in a vector form; ρ is the flux density; λ is any conserved characteristic for each element of the fluid; u, v, w are the zonal, meridional, and vertical velocity components; $f_h = 2\,\boldsymbol{\Omega}\cos\varphi$. Thus, due to the PV constancy, there is a close relationship between the absolute vorticity and static stability, which is caused by the action of the buoyancy force, i.e., vertical stratification of temperature and salinity (Winkler, R., Zwatz-Meise, V., 2001, Manual of synoptic satellite meteorology. Conceptual models and case studies. Version 6.8. http://www.zamg.ac.at/docu/Manual).

In the Boussinesq approximation, only the vertical component is considered, then expression (7) will take the following form (8):

$$PV = \frac{\zeta + f}{\rho}\frac{\partial \lambda}{\partial z}. \tag{8}$$

As mentioned earlier, λ is any conserved characteristic for each liquid element, for example, the potential density of water ρ (for the ocean) and the potential temperature (for the atmosphere) are often used. Thus, PV for the ocean will be calculated by the formula (9):

$$PV = \frac{\zeta + f}{\rho}\frac{\partial \rho}{\partial z}, \tag{9}$$

or, if we replace part of the expression with the Väisälä-Brunt frequency

$$N^2 = -\frac{g}{\rho}\frac{\partial \rho}{\partial z},$$

then:

$$PV = -\frac{1}{g}\left(f + \zeta\right) N^2. \tag{10}$$

Note that according to many practical works [*Bosse et al.,* 2019; *Smilenova et al.,* 2020; *Trodahl et al.,* 2020], a minus sign is presented in a formula (9) but is absent in formula (10) which, at a glimpse, somehow contradicts Ertel's theorem. However, if we consider that

$$\frac{D}{Dt}\left(PV\right) = 0,$$

i.e., $PV =$const, then the sign is irrelevant generally. The authors add it to make it easier to analyze positive values. Further, we will also give formulas with the opposite sign for calculating positive PV values. In this case, PV will be positive under the condition of a quiescent, stably stratified ocean in the northern hemisphere [*Bryan,* 1987].

Let us consider the variations of the calculation formulas encountered in practice. For example, in [*Smilenova et al.,* 2020], the following formula is used (11):

$$PV = \frac{1}{g}\left(f + \zeta\right) N^2 + \frac{1}{\rho}\left(\frac{\partial v}{\partial z}\frac{\partial \rho}{\partial x} - \frac{\partial u}{\partial z}\frac{\partial \rho}{\partial y}\right), \tag{11}$$

where g is the gravitational acceleration; u, v are the zonal and meridional velocity components.

In [*Bosse et al.,* 2019], formula (12) for polar coordinates is given:

$$PV\left(r, z\right) = \frac{1}{g}\left(f + \zeta\right) N^2 - \frac{1}{g}\frac{\partial v_\theta}{\partial z}\frac{\partial b}{\partial r}. \tag{12}$$

When we pass to Cartesian coordinates, the following formula (13) can be obtained:

$$PV = \frac{1}{g}\left(f + \zeta\right) N^2 - \frac{1}{g}\left(\frac{\partial v}{\partial z}\frac{\partial b}{\partial x} - \frac{\partial u}{\partial z}\frac{\partial b}{\partial y}\right), \tag{13}$$

where is the buoyancy force.

We performed calculations for 10 June 2010 using three formulas: (9), (11) (13). It was found that the results differ insignificantly from each other (on average, the difference is of the order of 10^{-13}), therefore for the Lofoten Basin conditions, it was expedient to use a simpler formula (9).

2.2. Selecting the Vortex Boundaries and Calculating Vortex Size

Currently, there is no standardized method for identifying the vortex boundaries. The most common methods are the selection by isopycnal/isothermal surfaces or by maximum velocities (gives underestimated vortex radius). In addition, it would be useful to consider the dynamic characteristics when identifying the vortex boundaries, therefore, the relative and potential vorticities can also be applied. It is worth remembering that the methods are very arbitrary, all criteria are determined empirically for a specific vortex, and in general, the obtained values (vortex volume, its vertical and horizontal dimensions) should be considered not as absolute values, but as relative values that reflect the temporal variability of a particular vortex.

The following empirical criteria were selected to isolate the LV: relative vorticity $\zeta < 5 \times 10^{-6}$ s^{-1} (Figure 3a–Figure 3d, yellow lines), potential vorticity $PV < 4{\times}10^{-11}$ m^{-1} s^{-1} (Figure 3a–Figure 3d, red lines). To cut off the region of small values located deeper than the lower vortex boundary, we also added the criterion of the potential density $\rho < 1027.96$ kg m^{-3} (Figure 3a–Figure 3d, blue lines). To calculate the potential density and the Väisälä-Brunt frequency required for the calculation, we used the thermodynamic equation of seawater TEOS-10 (http://www.teos-10.org/), implemented in the MATLAB programming language.

The area within 69–71°N and 1–6°E was considered. Then the masks of all areas satisfying the listed conditions were selected (Figure 3e–Figure 3f, yellow lines). What should we do if other anticyclonic eddies with fulfilled stated conditions are observed in the investigated area? In most cases, LV is much more intense than other anticyclonic eddies of the LB, i.e., has the highest negative relative

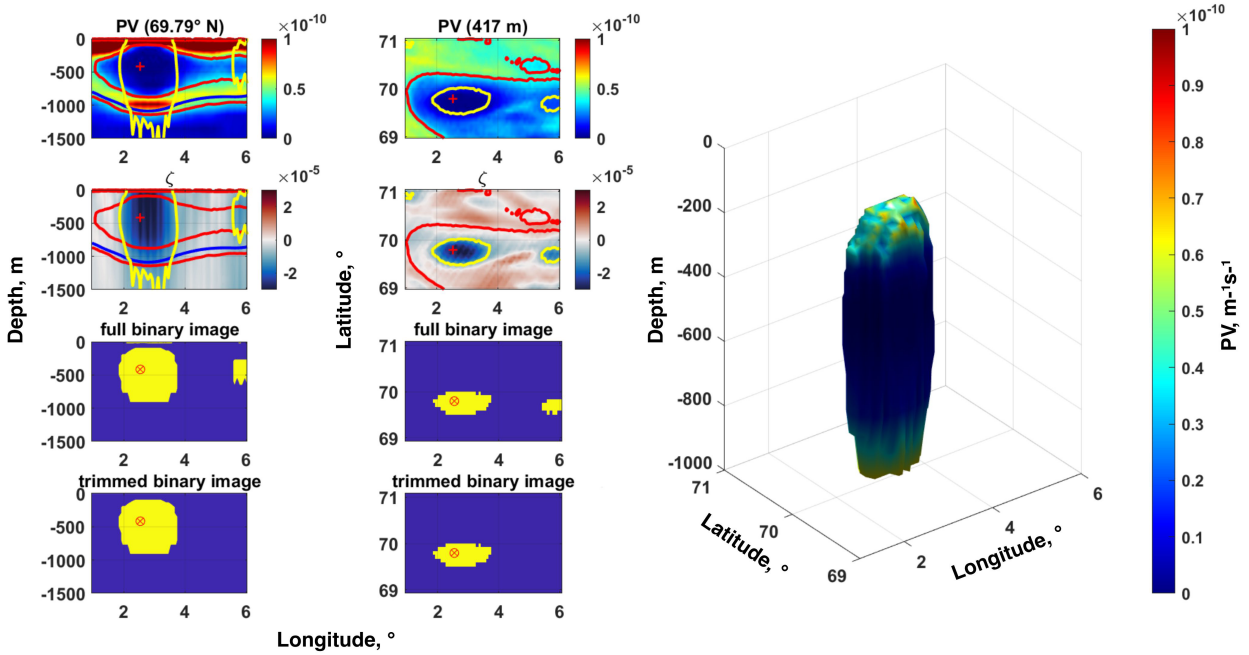

Figure 3. The potential vorticity (a, b), the relative vorticity (c, d), the mask of all areas satisfying the given conditions (e, f), Lofoten vortex mask (g, h) on the vertical (left side) and horizontal (right side) sections. The shape of the Lofoten vortex core (i), the potential vorticity is shown in color. The red cross marks the center of the Lofoten vortex. Figures are for October 2010 (monthly average).

vorticity. The minimum relative vorticity is usually observed in the surface layers; however, for most of the year (on average, 7–8 months), the vortex core is isolated from the surface. The articles [*Fer et al.,* 2018; *Travkin and Belonenko,* 2019; *Zinchenko et al.,* 2019] show that the cores of mesoscale eddies are usually located in the 300–600 m layer. For this reason, the point with the lowest relative vorticity at a depth of 417 m (approximately in the middle) was chosen as the center of the LV (Figure 3e–Figure 3h, red cross). In rare cases, when the smallest relative vorticity was observed outside the selected mask, the pairwise distance between this point and all other cells of the mask was determined, and then the cell located at the smallest distance was selected. It is important to note that the minimum relative vorticity is not always observed in the LV, therefore, it is necessary to verify at the appropriate stages of calculations. Next, the associated 3D areas were selected and labeled. Cells were combined into one area only if they had a common face; if the cells had only a common edge or vertex, they were distinguished as different areas. The LV was recognized as the area that contains the point previously defined as the center of the LV.

We also calculated the height and diameter of the vortex core. The vortex diameter was determined at each horizon by approximating its boundary with a circle (Bucher, I., 2021, Circle fit, MATLAB Central File Exchange. https://www.mathworks.com/matlabcentral/fileexchange/5557-circle-fit), and then the largest diameter was chosen. The core height was determined by the difference between the minimum and maximum depth where the vortex was recorded. The vortex volume was calculated as the sum of each cell volume where the vortex was determined. The cell volume was found as the product of its base area (the area of the corresponding grid cell with a size of $0.083° \times 0.083°$) by the height of the cell.

3. Data

The global ocean reanalysis GLORYS12V1 was used to calculate the potential density, orbital velocities, as well as relative and potential vortici-

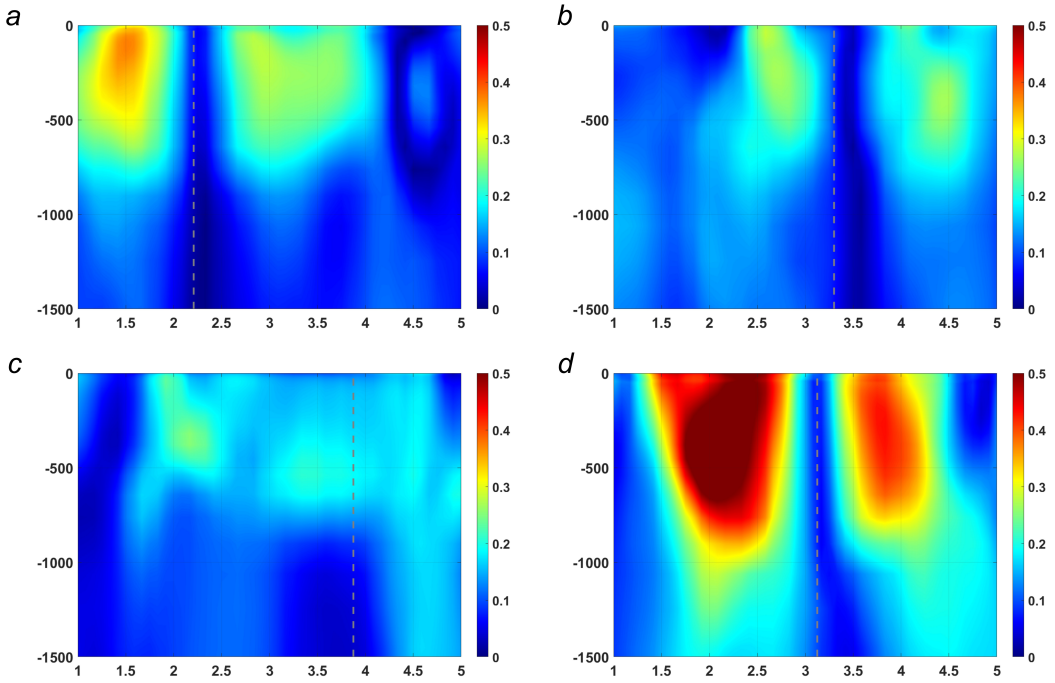

Figure 4. The vertical sections of the orbital velocity (m s^{-1}) in the Lofoten vortex on 1 September 2009 (a), 1 December 2009 (b), 1 March 2010 (c), and 1 June 2010 (d). The dotted line indicates the vortex center.

Table 1. Coordinates of the Lofoten Vortex Center

Date	Latitude	Longitude
1 September 2009	69.9583	2.2083
1 December 2009	69.9583	3.3000
1 March 2010	69.7083	3.8750
1 June 2010	69.8750	3.1250

ties. It is primarily based on the modern global real-time forecasting system Copernicus Marine Environment Monitoring Service (CMEMS). The model component is the NEMO platform and the ECMWF ERA-Interim reanalysis of surface characteristics. The data was downloaded from the Copernicus Marine Environment Monitoring Service website. The data are gridded and implemented in the WGS-84 coordinate system in the Mercator projection. Reanalysis has two types of temporal resolution: daily average and monthly average. There are also two spatial resolutions: 0.25° and 0.083°. The array GLOBAL-REANALYSIS-PHY-001-030-MONTHLY was chosen, which is monthly average data with a spatial resolution of 0.083° (∼ 8 km) and 50 vertical levels (from ∼ 0.5 to ∼ 5728 m). It covers the period from 1993 to 2019. The reanalysis includes water temperature (T), salinity (S), current velocity components (u, v), mixed layer depth, sea surface height and sea ice cover data (concentration, thickness, u and v drift components). Bathymetry data were taken from the global relief model of Earth's surface ETOPO1 [*Amante and Eakins,* 2009]. It is implemented on the 1/60° grid and includes the bottom topography. ETOPO1 is vertically referenced to sea level and horizontally referenced to the World Geodetic System of 1984 (WGS 84).

4. Results

Let us consider the seasonal variability of the LV characteristics according to the ocean reanalysis GLORYS12V1 using the 2009–2010 years example, when anomalously winter convection up to 1000 m was observed in the eddy region according

to ARGO data [*Fedorov et al.,* 2019, 2021]. We will use the calculations for 1 September 2009, 1 December 2009, 1 March 2010, and 1 June 2010 in the area bounded by 69–71°N, 1–5°E (Figure 1, black rectangle). Vertical sections are oriented zonally and drawn through the LV center (Table 1).

Figure 4 shows the vertical sections of orbital velocities in the LV. In autumn, the orbital velocities in the anticyclone doesn't get more than 37 cm s^{-1}. By winter, the speed decreases to 28 cm^{-1} and reaches their minimum in spring (25 cm^{-1} or less). In summer, the speed in the anticyclone is at its maximum and exceeds 50 cm^{-1}.

In September (Figure 5a) there is a pycnocline with a strong gradient. At a depth of 500–750 m, the isopycnals are bowl-shaped, which is due to the well-formed lenticular vortex core and, accordingly, the mixed waters inside it. Convection begins in the LV in November–December [*Bloshkina and Ivanov,* 2016; *Fedorov et al.,* 2019; *Richards and Straneo,* 2015; *Travkin and Belonenko,* 2020; *Voet et al.,* 2010], and the mixed layer in the LV center gradually reaches the surface. As a result, the mixed layer depth is about 200–250 m in the LV area in December (Figure 5b), and it exceeds 600 m in March (Figure 5c) when convection reaches its peak. The thermocline reappears in June (Figure 5d), as a result, the vortex lens loses connection with the surface. The vortex core is clear and compressed horizontally, because of which the orbital velocity increases, noted earlier in Figure 5d). In general, the change in thermohaline characteristics is mainly observed in the layer up to 1000 m, which is consistent with the results of the article [*Sandalyuk et al.,* 2020].

The relative vorticity is determined by the vertical component of the curl of the velocity vector, and the dynamic vortex signal is traced to the bottom during the year. This fact is also noted in the article [*Volkov et al.,* 2013]. In Figure 6a, it can be seen that in September the maximum values of the relative vorticity are located in a layer limited by 700 m, below which there is an isopycnals thickening. A more explicit isopycnals thickening is observed in the surface layer. In winter (Figure 6b), the vortex gradually weakens, the rotation slows down but spreads over larger distances. In March (Figure 6c), when convection reaches its peak [*Fedorov et al.,* 2019], the vortex is weakly expressed, it regularly disintegrates, there are no clear boundaries, the negative relative vorticity is small, but occupies large areas. Wherein, a relatively intense rotation penetrates to a greater depth (up to $\sim$ 700 m). The vortex compresses again in April, the relative vorticity increases, and by June (Figure 6d) the relative vorticity takes maximum in absolute values, which reach a depth of 1000–1100 m. It is important to note that, in general, the vortex dynamic signal is traced to the bottom during the year.

Let us consider the seasonal variability of Ertel's potential vorticity (Figure 7). In September (Figure 7a) the vortex is well developed, the vortex core is isolated from the surface, then in this case (1 September 2009), a dual-core structure is observed. Due to the strong anticyclonic vorticity and weak stratification, the potential vorticity in the vortex center is 3–4 orders of magnitude less than at the periphery ($10^{-14} - 10^{-13}$ in the vortex center versus 10^{-10} at the periphery). This PV distribution creates a barrier that prevents lateral exchange between the vortex core and the external environment [*Bosse et al.,* 2019; *Dugstad et al.,* 2021], as well as contributes to the turbulent diffusion suppression [*Bashmachnikov et al.,* 2015, 2017b; *Hua et al.,* 2013]. The presence of the barrier around the LV was also confirmed by ship data and RAFOS buoys data [*Bosse et al.,* 2019]. In contrast to the surface, where regular destruction/formation of a PV-barrier occurs, the layer of increased PV values at the lower vortex edge is relatively stable throughout the year and is observed on average at a depth of 700 to 1100 meters. From the third decade of November to December (Figure 7b), as a result of convective processes onset, the seasonal thermocline destroys, the barrier weakens, and lateral mixing and heat flux between the eddy and the environment increase, apparently due to dynamic instability and possible eddies merge [*Bosse et al.,* 2019]. The layer of increased PV-values between the surface and the vortex core completely disappears from the end of

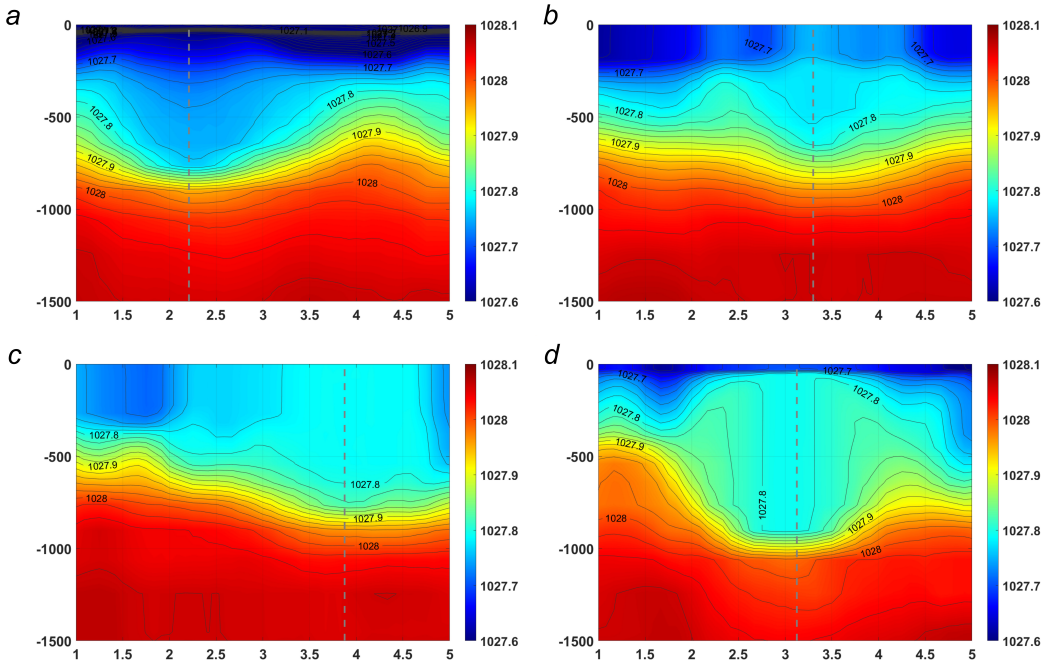

Figure 5. The vertical sections of the potential density in the Lofoten vortex on 1 September 2009 (a), 1 December 2009 (b), 1 March 2010 (c), and 1 June 2010 (d). The isopycnals are plotted with the lines, the dotted line indicates the vortex center.

February to March (Figure 7c). It indicates an active interaction with the atmosphere and enhanced heat transfer, which creates favorable conditions for its convective regeneration [*Alexeev et al.,* 2016]. The layer of increased PV-values between the surface and the vortex reappears in the second half of May, when the surface water begins to warm up and the seasonal thermocline begins to form, the homogeneous core loses its connection with the surface and takes on a lenticular shape. The vortex is fully formed by June (Figure 7d), it shrinks and reaches its maximum intensity. During the summer, due to the absence of new portions of water from the surface [*Alexeev et al.,* 2016], the horizontal density gradient at the lens boundaries weakens, which leads to a slowdown in rotation, its compression vertically and stretching horizontally.

Next, we calculated the relative volume of the LV core, the minimum relative vorticity, and the average potential vorticity in the vortex core, as well as the vertical and horizontal dimensions of the vortex (Figure 8).

The maximum vortex height is observed in winter (Figure 8g, Figure 8h), during the winter convection, when the thermocline is destroyed, and the vortex comes to the surface. In summer, when the thermocline is formed, the vortex spreads over large horizontal distances, its diameter reaches maximum values (Figure 8i, Figure 8j). If the "ice skater effect" (see Section 2.1) works for this situation, there should be a vortex intensification in winter and its relaxation in summer. The authors of the article [*Ivanov and Korablev,* 1995b] come to the same conclusion. However, if we pay attention to the distribution of the relative vorticity throughout the year (Figure 8c, Figure 8d), it will be found that the lowest velocities are observed in March, and the highest values are achieved from late summer to early autumn. Probably, this "effect" is not the general case since there is an active interaction of the vortex with the atmosphere in winter. When the vortex was isolated from the surface, i.e., when the upper and lower vortex boundaries were determined mainly by the given PV-surfaces, a close relationship was found between the vortex height and its intensity (relative vorticity) (Figure 9b), the correlation is 0.62. The correlation between the diameter and intensity of the vortex is insignificant

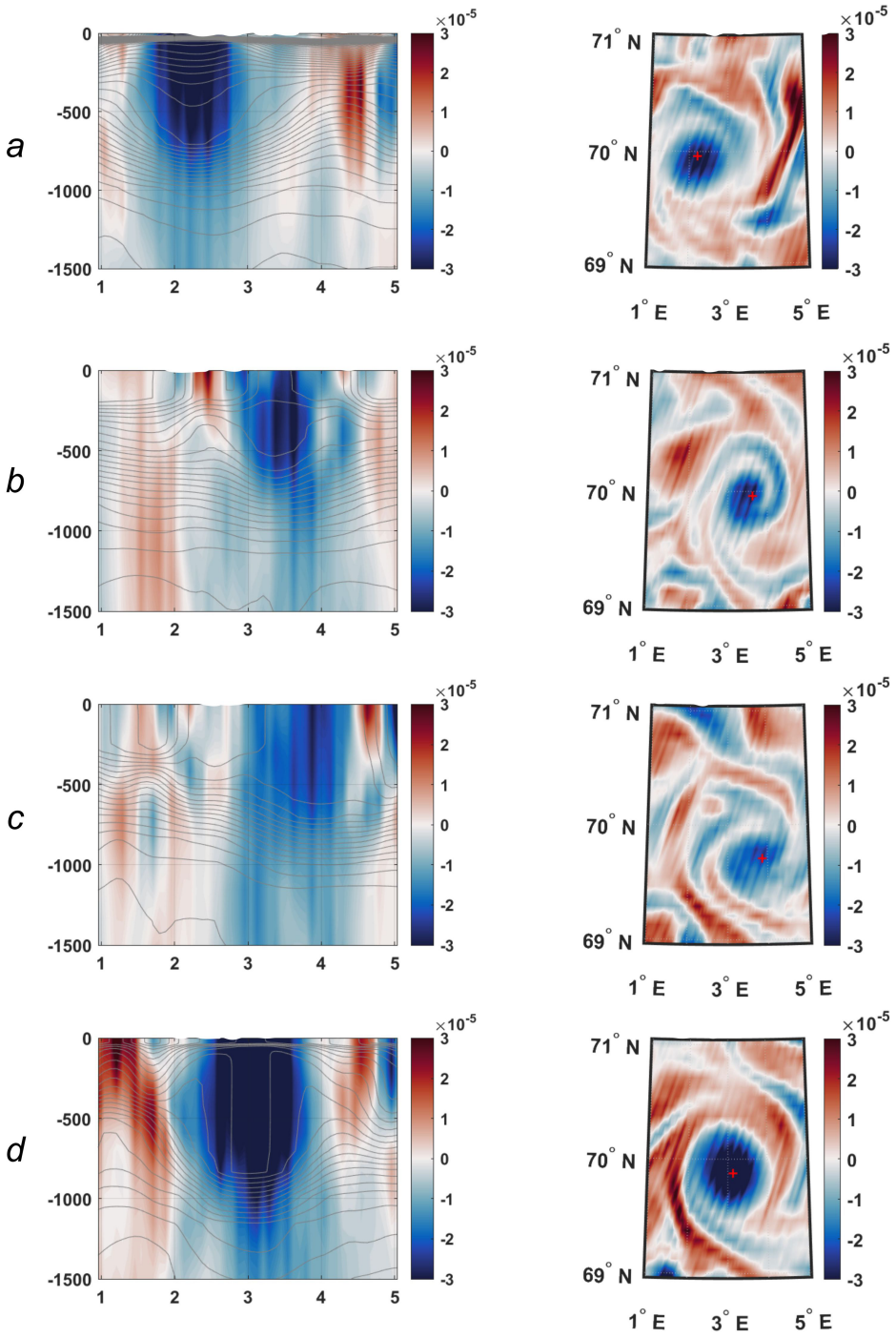

Figure 6. The distribution of the relative vorticity (ζ) on the vertical sections (left) and at a depth of 417 m (right) on 1 September 2009 (a), 1 December 2009 (b), 1 March 2010 (c), and 1 June 2010 (d). The isopycnals are plotted with the lines.

(0.13 – for a subsurface vortex; 0.19 – for a surface vortex). This is probably due to the lateral vortex boundaries being distinguished mainly by the relative vorticity instead of potential vorticity.

The correlation (Figure 9a) between the volume of the LV core (Figure 8a, Figure 8b) and the largest absolute relative vorticity value inside the core (Figure 8c, Figure 8d) is −0.65. When the

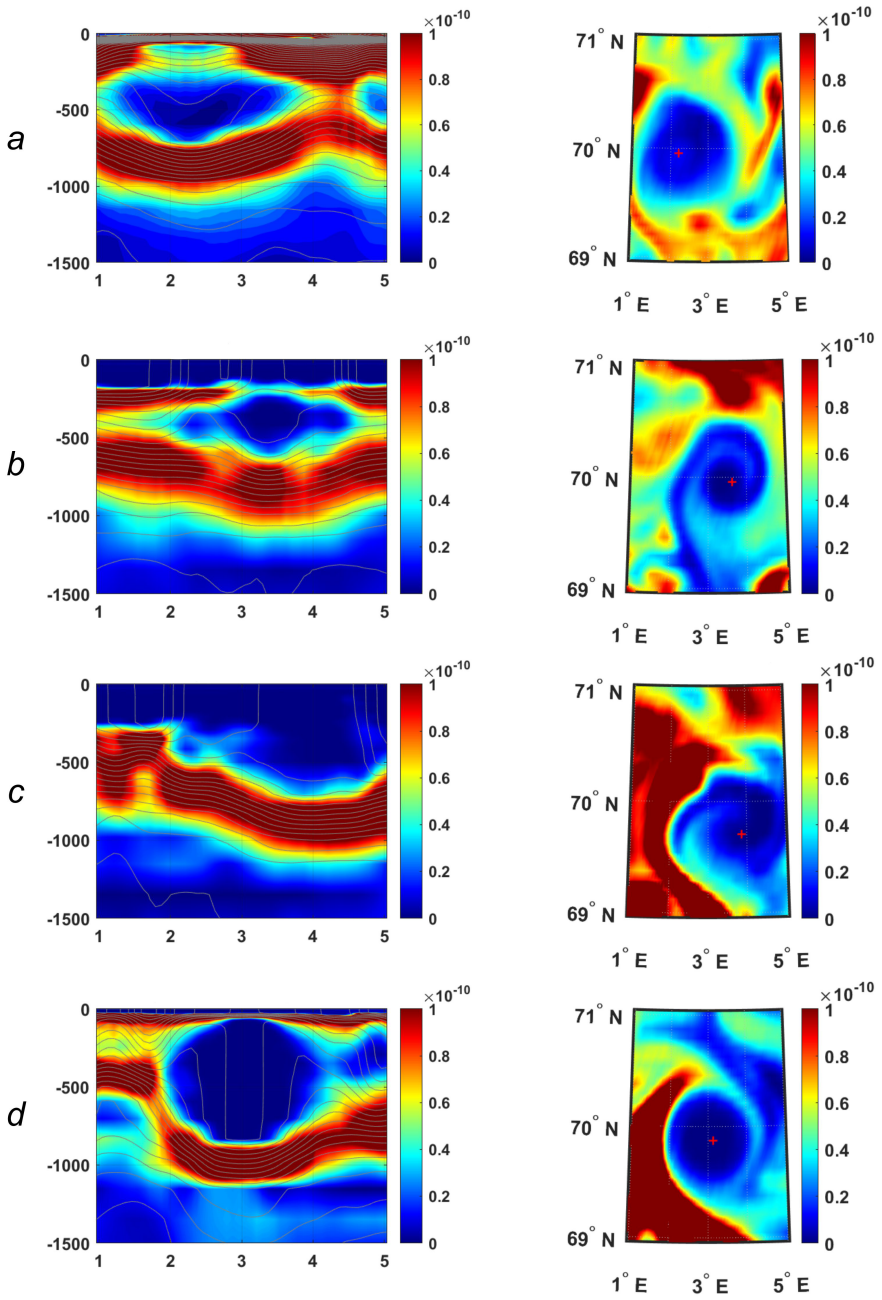

Figure 7. The distribution of the potential vorticity (PV) on the vertical sections (left) and at a depth of 417 m (right) on 1 September 2009 (a), 1 December 2009 (b), 1 March 2010 (c), and 1 June 2010 (d). The isopycnals are plotted with the lines.

core is isolated from the surface and there is no interaction with the atmosphere, the correlation is slightly higher and reaches −0.69; on contact with the surface, the correlation is −0.60. Figure 9a shows that for small LV sizes, it has a constantly low intensity, while large sizes allow for a larger intensity variability. Thus, when the LV had the largest size (1.77×10^{13} m^3), its relative vorticity was only -2.54×10^{-5} s^{-1}.

When the vortex is isolated from the surface, the vortex volume (Figure 8a, Figure 8b) correlates well with the average potential vorticity (Fig-

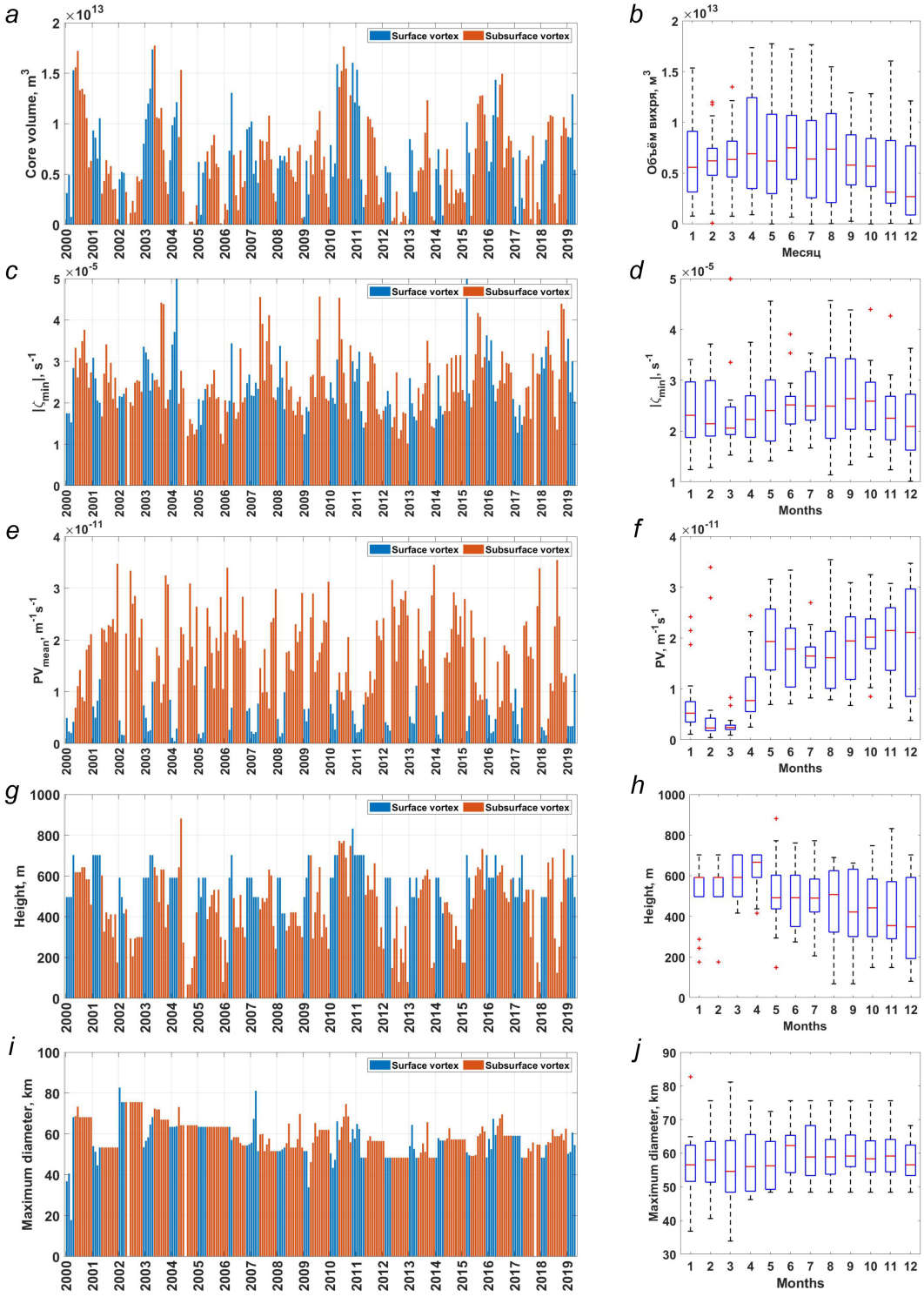

Figure 8. The time courses (left) and box plots (right) of the Lofoten vortex volume (a, b), its minimum relative vorticity (c, d), average potential vorticity (e, f), vortex core height (g, h), and maximum vortex diameter (i, j). On the time courses, blue shows the months when the vortex core was in contact with the surface, orange – when the core was below the surface. On the box plots, the center red mark represents the median, and the bottom and top edges of the box represent the 25th and 75th percentiles; the whiskers are drawn to the extreme not considered outliers; outliers are marked with a red cross.

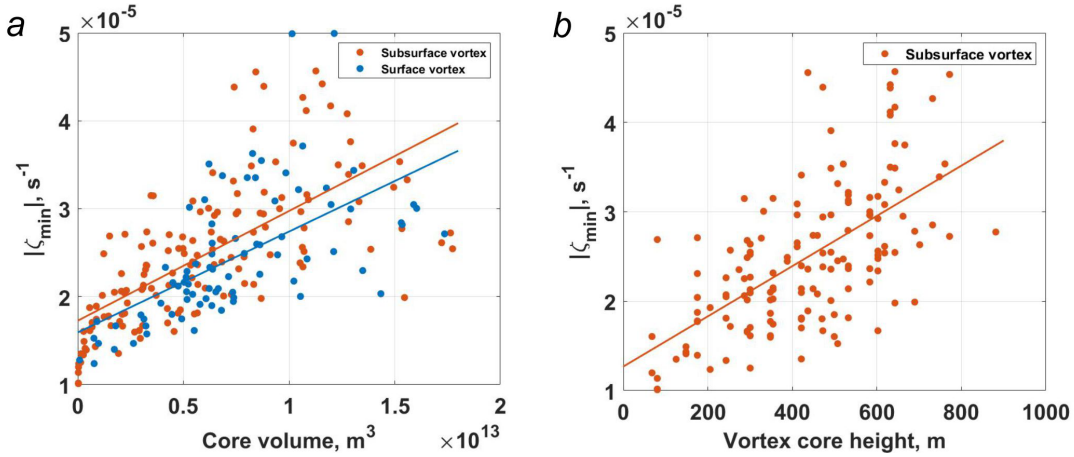

Figure 9. The dependence between the minimum relative vorticity and the volume of the Lofoten vortex core (a); dependence between the minimum relative vorticity and the vortex core height (b).

ure 8e, Figure 8f) inside it, the correlation is −0.72 (not shown). However, in the case when the vortex reaches the surface, there is no correlation.

5. Discussions and Conclusions

The anticyclonic Lofoten vortex is a strong dynamic formation, the dynamic signal of which spreads to the bottom, and the change in thermohaline characteristics is mainly observed in the layer up to 1000 m. We expected that when the vortex is stretching vertically, its intensity (absolute value of relative vorticity and orbital velocity) would be the greatest, and, on the contrary, when the vortex is spreading, the relative vorticity should also decrease. This corresponds to general physical concepts but is not always the case. The highest eddy height is observed in winter when the relative vorticity is minimal. This is due to the thermocline destruction and the vortex emergence to the surface; therefore, it actively interacts with the atmosphere, i.e., the conservation law is not fulfilled [*Zhmur et al.,* 2021a, 2021b, 2022]. If we consider the case when the vortex is isolated from the surface, i.e., when both its vertical boundaries are determined by the given PV-surfaces, the highest vortex height corresponds to its highest intensity. The correlation is 0.62. At the same time, there is no connection between the vortex diameter and its intensity. According to our calculations, the vortex diameter does not change much during the year, the largest vortex diameter is observed in the summer – during the period of the maximum vortex intensity. The absence of a connection between the vortex intensity and its diameter may be due to the lateral vortex boundaries that are distinguished by the relative vorticity (not by the potential) to close the selected area.

Surprisingly, the vortex intensifies not during the winter convection, which is one of the reasons for its regeneration, but in summer. Although the vortex intensification in the winter period is discussed in the article [*Ivanov and Korablev,* 1995a], the field studies of the authors are limited to the summer period and are not concerned with the assessment of the vortex intensity. Our analysis showed that vortex relaxation occurs in winter, and its intensification is in summer.

Acknowledgments. The authors acknowledge the support of the Russian Science Foundation (RSF, project No. 22-27-00004).

References

Alexeev, V. A., V. V. Ivanov, et al. (2016), Convective structures in the Lofoten Basin based on satellite and Argo data, *Izvestiya, Atmospheric and Oceanic Physics*, *52,* No. 9, 1064–1077, **Crossref**

Allen, J. T., D. A. Smeed (1996), Potential Vorticity and Vertical Velocity at the Iceland-Færoes Front, *Journal of Physical Oceanography*, *26,* No. 12, 2611–2634, **Crossref**

Amante, C., B. W. Eakins (2009), *ETOPO1 1 Arc-Minute Global Relief Model: Procedures, Data Sources and Analysis*, NOAA, National Geophysical Data Center, Boulder. **Crossref**

Bashmachnikov, I. L., T. V. Belonenko, P. A. Kuibin (2017a), Application of the theory of columnar Q-vortices with helical structure for the Lofoten Vortex of the Norwegian sea, *Vestnik Sankt-Peterburgskogo Universiteta. Nauki o Zemle*, *62,* No. 3, 221–236, (in Russian)**Crossref**

Bashmachnikov, I. L., F. Neves, et al. (2015), Properties and pathways of Mediterranean water eddies in the Atlantic, *Progress in Oceanography*, *137,* 149–172, **Crossref**

Bashmachnikov, I. L., et al. (2017b), On the vertical structure and stability of the Lofoten vortex in the Norwegian Sea, *Deep-Sea Research Part I: Oceanographic Research Papers*, *128,* 1–27, **Crossref**

Belonenko, T. V., I. L. Bashmachnikov, et al. (2017), On the vertical velocity component in the mesoscale Lofoten vortex of the Norwegian Sea, *Izvestiya, Atmospheric and Oceanic Physics*, *53,* No. 6, 641–649, **Crossref**

Belonenko, T. V., A. V. Koldunov, et al. (2018), Thermohaline structure of the Lofoten vortex in the Norwegian sea based on field research and hydrodynamic modeling, *Vestnik Sankt-Peterburgskogo Universiteta. Nauki o Zemle*, *63,* No. 4, 502–519, (in Russian)**Crossref**

Belonenko, T. V., V. S. Travkin, et al. (2021), Topographic experiments over dynamical processes in the Norwegian Sea, *Russian Journal of Earth Sciences*, *21,* ES1006, **Crossref**

Belonenko, T. V., D. L. Volkov, et al. (2014), Circulation of waters in the Lofoten Basin of the Norwegian Sea, *Vestnik Sankt-Peterburgskogo Universiteta. Nauki o Zemle*, *7,* No. 2, 108–121. (in Russian)

Bloshkina, E. V., V. V. Ivanov (2016), Convective structures in the Norwegian and Greenland Seas based on simulation results with high spatial resolution, *Proceedings of the Hydrometeorological Research Center of the RF*, *361,* 146–168. (in Russian)

Bosse, A., I. Fer, et al. (2019), Dynamical controls on the longevity of a non-linear vortex: The case of the Lofoten Basin Eddy, *Scientific Reports*, *9,* No. 1, 1–13, **Crossref**

Bosse, A., I. Fer, et al. (2018), Atlantic Water Transformation Along Its Poleward Pathway Across the Nordic Seas, *Journal of Geophysical Research: Oceans*, *123,* No. 9, 6428–6448, **Crossref**

Bryan, K. (1987), Potential vorticity in models of the ocean circulation, *Quarterly Journal of the Royal Meteorological Society*, *113,* No. 477, 713–734, **Crossref**

Catling, D. C. (2015), Planetary Atmospheres, *Treatise on Geophysics (2nd ed.), G. Schubert (Ed.)* p. 429–472, Elsevier, Oxford. **Crossref**

Chelton, D. B., R. A. de Szoeke, M. G. Schlax (1998), Geographical Variability of the First Baroclinic Rossby Radius of Deformation, *Journal of Physical Oceanography*, *28,* 433–460, **Crossref**

Dugstad, J. S., P. E. Isachsen, I. Fer (2021), The mesoscale eddy field in the Lofoten Basin from high-resolution Lagrangian simulations, *Ocean Science*, *17,* No. 3, 651–674, **Crossref**

Ertel, H. (1942a), Ein neuer hydrodynamischer Erhaltungssatz, *Die Naturwissenschaften*, *30,* 543–544, **Crossref**

Ertel, H. (1942b), Ein neuer hydrodynamischer Wirbelsatz, *Meteorologische Zeitschrift*, *59,* 277–281.

Ertel, H. (1942c), Über hydrodynamischer Wirbelsätze, *Physikalische Zeitschrift Leipzig*, *43,* 526–529.

Fedorov, A. M., I. L. Bashmachnikov, T. V. Belonenko (2019), Winter convection in the Lofoten Basin according to ARGO buoys and hydrodynamic modeling, *Vestnik Sankt-Peterburgskogo Universiteta. Nauki o Zemle*, *64,* No. 3, 491–511, (in Russian)**Crossref**

Fedorov, A. M., T. V. Belonenko (2020), Interaction of mesoscale vortices in the Lofoten Basin based on the GLORYS database, *Russian Journal of Earth Sciences*, *20,* No. 2, ES2002, **Crossref**

Fedorov, A. M., R. P. Raj, et al. (2021), Extreme Convective Events in the Lofoten Basin, *Pure and Applied Geophysics*, *178,* 2379–2391, **Crossref**

Fer, I., A. Bosse, et al. (2018), The dissipation of kinetic energy in the Lofoten Basin Eddy, *Journal of Physical Oceanography*, *48,* No. 6, 1299–1316, **Crossref**

Gordeeva, S. M., V. A. Zinchenko, et al. (2020), Statistical analysis of long-lived mesoscale eddies in the Lofoten basin from satellite altimetry, *Advances in Space Research*, *68,* No. 2, 364–377, **Crossref**

Hua, B. L., C. Ménesguen, et al. (2013), Layering and turbulence surrounding an anticyclonic oceanic vortex: in situ observations and quasi-geostrophic numerical simulations, *Journal of Fluid Mechanics*, *731,* 418–442, **Crossref**

Ivanov, V. V., A. A. Korablev (1995a), Dynamics of an intrapycnocline lens in the Norwegian Sea, *Russ. Meteorol. Hydrol.*, No. 10, 32–37. (in Russian)

Ivanov, V. V., A. A. Korablev (1995b), Formation and regeneration of the pycnocline lens in the Norwegian Sea, *Russ. Meteorol. Hydrol.*, No. 9, 62–69. (in Russian)

Köhl, A. (2007), Generation and stability of a quasi-permanent vortex in the Lofoten Basin, *Journal of Physical Oceanography*, *37,* No. 11, 2637–2651, **Crossref**

Koszalka, I., J. H. LaCasce, et al. (2011), Surface circulation in the Nordic Seas from clustered drifters, *Deep-Sea Research Part I: Oceanographic Research Papers*, *58,* No. 4, 468–485, **Crossref**

Kushner, P. J. (2003), Circulation, Vorticity, and Potential Vorticity, *Handbook of Weather, Climate, and Water: Dynamics, Climate, Physical Meteorology, Weather Systems, and Measurements, T. D. Potter & B. R. Colman (Eds.)* p. 21–38, John Wiley & Sons, Inc., Hoboken. **Crossref**

Nilsen, J. E. Ø., E. Falck (2006), Variations of mixed layer properties in the Norwegian Sea for the period 1948–1999, *Progress in Oceanography*, *70,* No. 1, 58–90, **Crossref**

Novoselova, E. V., T. V. Belonenko (2020), Isopycnal Advection in the Lofoten Basin of the Norwegian Sea, *Fundamentalnaya i Prikladnaya Gidrofizika*, *13,* No. 3, 56–67, (in Russian)**Crossref**

Novoselova, E. V., T. V. Belonenko, V. G. Gnevyshev (2020), The baroclinic Rossby radius in the Nordic seas, *Sovremennye Problemy Distantsionnogo Zondirovaniya Zemli Iz Kosmosa*, *17,* No. 5, 228–240, (in Russian)**Crossref**

Pidcock, R., A. Martin, et al. (2013), The spatial variability of vertical velocity in an Iceland basin eddy dipole, *Deep-Sea Research Part I: Oceanographic Research Papers*, *72,* 121–140, **Crossref**

Raj, R. P., L. Chafik, et al. (2015), The Lofoten Vortex of the Nordic Seas, *Deep-Sea Research Part I: Oceanographic Research Papers*, *96,* 1–14, **Crossref**

Raj, R. P., I. Halo, et al. (2020), Interaction Between Mesoscale Eddies and the Gyre Circulation in the Lofoten Basin, *Journal of Geophysical Research: Oceans*, *125,* No. 7, e2020JC016102, **Crossref**

Richards, C. G., F. Straneo (2015), Observations of water mass transformation and eddies in the Lofoten basin of the Nordic seas, *Journal of Physical Oceanography*, *45,* No. 6, 1735–1756, **Crossref**

Rossby, C.-G. (1936), *Dynamics of Steady Ocean Currents in the Light of Experimental Fluid Mechanics (Vol. 5)*, Massachusetts Institute of Technology and Woods Hole Oceanographic Institution, Massachusetts. **Crossref**

Rossby, C.-G. (1938), On the mutual adjustment of pressure and velocity distributions in certain simple current systems, II, *Journal of Marine Research*, *1,* No. 3, 239–263, **Crossref**

Rossby, C.-G. (1940), Planetary flow patterns in the atmosphere, *Quarterly Journal of the Royal Meteorological Society*, *66,* 68–87. (Retrieved from http://www.aos.princeton.edu/WWWPUBLIC/gkv/history/Rossby-planflowQJ40.pdf)

Rossby, C.-G., V. K. Ozhigin, et al. (2009a), An isopycnal view of the Nordic Seas hydrography with focus on properties of the Lofoten Basin, *Deep-Sea Research Part I: Oceanographic Research Papers*, *56,* No. 11, 1955–1971, **Crossref**

Rossby, T., M. D. Prater, H. Søiland (2009b), Pathways of inflow and dispersion of warm waters in the Nordic seas, *Journal of Geophysical Research: Oceans*, *114,* No. 4, 1–17, **Crossref**

Samelson, R. M. (2003), *Rossby, Ertel, and Potential Vorticity*, Oregon University, Corvallis.

Sandalyuk, N. V., A. Bosse, T. V. Belonenko (2020), The 3-D Structure of Mesoscale Eddies in the Lofoten Basin of the Norwegian Sea: A Composite Analysis From Altimetry and In Situ Data, *Journal of Geophysical Research: Oceans*, *125,* No. 10, e2020JC016331, **Crossref**

Santeva, E. K., I. L. Bashmachnikov, M.A. Sokolovskiy (2021), On the Stability of the Lofoten Vortex in the Norwegian Sea, *Oceanology*, *61,* No. 3, 308–318, **Crossref**

Schubert, W., E. Ruprecht, et al. (2004), English translations of twenty-one of Ertel's papers on geophysical fluid dynamics, *Meteorologische Zeitschrift*, *13,* No. 6, 527–576, **Crossref**

Smilenova, A., J. Gula, et al. (2020), A Persistent Deep Anticyclonic Vortex in the Rockall Trough Sustained by Anticyclonic Vortices Shed From the Slope Current and Wintertime Convection, *Journal of Geophysical Research: Oceans*, *125,* No. 10, 1–27, **Crossref**

Søiland, H., T. Rossby (2013), On the structure of the Lofoten Basin Eddy, *Journal of Geophysical Research: Oceans*, *118,* No. 9, 4201–4212, **Crossref**

Søiland, H., L. Chafik, T. Rossby (2016), On the long-term stability of the Lofoten Basin Eddy, *Journal of Geophysical Research: Oceans*, *121,* No. 7, 4438–4449, **Crossref**

Spall, M. A. (2010), Non-local topographic influences on deep convection: An idealized model for the Nordic Seas, *Ocean Modelling*, *32,* No. 1–2, 72–85, **Crossref**

Steele, J. H., K. K. Turekian, S. A. Thorpe, (Eds.) (2001), Non-local topographic influences on deep convection: An idealized model for the Nordic Seas, *Ocean Modelling*, **Crossref**

Stewart, R. H. (2008), *Introduction to Physical Oceanography*, Texas A&M University, Texas.

Talley, L. D., G. L. Pickard, et al. (2011), Dynamical Processes for Descriptive Ocean Circulation, *Ocean Modelling*, 187–221, **Crossref**

Travkin, V. S., T. V. Belonenko (2019), Seasonal variability of mesoscale eddies of the Lofoten Basin using satellite and model data, *Russian Journal of Earth Sciences*, *19,* No. 5, ES5004, **Crossref**

Travkin, V. S., T. V. Belonenko (2020), Mixed layer depth in winter convection in the Lofoten Basin in the Norwegian Sea and assessment methods, *Hydrometeorology and Ecology, Proceedings of the Russian State Hydrometeorological University*, *59,* 67–83, (in Russian)**Crossref**

Trodahl, M., P. E. Isachsen, et al. (2020), The regeneration of the lofoten vortex through vertical alignment, *Journal of Physical Oceanography*, *50,* No. 9, 2689–2711, **Crossref**

Vallis, G. K. (2006), *Atmospheric and Oceanic Fluid Dynamics: Fundamentals and Large-scale Circulation*, Cambridge University Press, New York. **Crossref**

Voet, G., D. Quadfasel, et al. (2010), The mid-depth circulation of the Nordic Seas derived from profiling float observations, *Tellus, Series A: Dynamic Meteorology and Oceanography*, *62,* No. 4, 516–529, **Crossref**

Volkov, D. L., T. V. Belonenko, V. R. Foux (2013), Puzzling over the dynamics of the Lofoten Basin – a sub-Arctic hot spot of ocean variability, *Geophysical Research Letters*, *40,* No. 4, 738–743, **Crossref**

Volkov, D. L., A. A. Kubryakov, R. Lumpkin (2015), Formation and variability of the Lofoten basin vortex in a high-resolution ocean model, *Deep-Sea Research Part I: Oceanographic Research Papers*, *105,* 142–157, **Crossref**

Ypma, S. L., S. Georgiou, et al. (2020), Pathways and Water Mass Transformation Along and Across the Mohn-Knipovich Ridge in the Nordic Seas, *Journal of Geophysical Research: Oceans*, *125,* **Crossref**

Yu, L.-S., A. Bosse, et al. (2017), The Lofoten Basin eddy: Three years of evolution as observed by Seagliders, *Journal of Geophysical Research: Oceans*, *122,* No. 8, 6814–6834, **Crossref**

Zhmur, V. V., E. V. Novoselova, T. V. Belonenko (2021a), Features of the formation of the density field in the mesoscale eddies of the Lofoten basin. Part 1, *Oceanology*, *61,* 830–838, **Crossref**

Zhmur, V. V., E. V. Novoselova, T. V. Belonenko (2021b), Potential vorticity in the ocean: Ertel and Rossby approaches with estimates for the Lofoten vortex, *Izvestiya, Atmospheric and Oceanic Physics*, *57,* No. 6, 632–641, **Crossref**

Zhmur, V. V., E. V. Novoselova, T. V. Belonenko (2022), Features of the formation of the density field in the mesoscale eddies of the Lofoten basin. Part 2, *Oceanology*, *62,* No. 3, 341–356, **Crossref**

Zinchenko, V. A., S. M. Gordeeva, et al. (2019), Analysis of Mesoscale eddies in the Lofoten Basin based on satellite altimetry, *Fundamentalnaya i Prikladnaya Gidrofizika*, *12,* No. 3, 46–54, **Crossref**

Corresponding author:
Elena V. Novoselova, St. Petersburg State University, St. Petersburg, Russia. (novoselovaa.elena@gmail.com)